

# Mechanotargeting: Mechanics-Dependent Cellular Uptake of Nanoparticles

Qiong Wei, Changjin Huang, Yao Zhang, Tiankai Zhao, Peng Zhao, Peter Butler, and Sulin Zhang\*

**Targeted delivery of nanoparticle (NP)-based diagnostic and therapeutic agents to malignant cells and tissues has exclusively relied on chemotargeting, wherein NPs are surface-coated with ligands that specifically bind to overexpressed receptors on malignant cells. Here, it is demonstrated that cellular uptake of NPs can also be biased to malignant cells based on the differential mechanical states of cells, enabling mechanotargeting. Owing to mechanotransduction, cell lines (HeLa and HCT-8) cultured on hydrogels of various stiffness are directed into different stress states, measured by cellular force microscopies. In vitro NP delivery reveals that increases in cell stress suppress cellular uptake, counteracting the enhanced uptake that occurs with increases in exposed surface area of spread cells. Upon prolonged culture on stiff hydrogels, cohesive HCT-8 cell colonies undergo metastatic phenotypic change and disperse into individual malignant cells. The metastatic cells are of extremely low stress state and adopt an unspread, 3D morphology, resulting in several-fold higher uptake than the nonmetastatic counterparts. This study opens a new paradigm of harnessing mechanics for the design of future strategies in nanomedicine.**

Enormous efforts over the last several decades have been undertaken toward developing multifunctional nanoparticles (NPs) as the next-generation medicine that allows early-stage cancer detection, and simultaneous diagnosis and treatment of pathological conditions.<sup>[1–3]</sup> To improve targeting efficiency and reduce nonspecific delivery, cellular uptake of NPs must bias toward malignant cells. Chemotargeting,<sup>[4–6]</sup> the primary targeting strategy to date, relies on specific binding of the ligands coated on NP surface to the surface receptors overexpressed on malignant cells. In contrast to the weak nonspecific interactions such as van der Waals and electrostatic interactions,

the ligand–receptor pair forms a molecular “lock-and-key” system and provides high adhesion energy that drives cellular uptake,<sup>[7]</sup> enabling targeting specificity and selectivity. However, clinical application of NPs in cancer imaging and therapy is still hampered by a series of issues, including insufficient uptake by tumors, low accessibility to cancer cells, and high nonspecific uptake by the liver and other organs.<sup>[8,9]</sup> Therefore, it remains an imperative challenge to develop NP-based targeted therapies with improved targeting efficiency and minimized toxicity.


Recent theoretical studies have revealed that surface mechanics of cells, including cell membrane bending and membrane tension, also mediates cellular uptake of NPs.<sup>[10–13]</sup> During endocytosis, cell membrane invaginates the NP, and pinches it off to deliver it into the cell. The invagination process involves membrane

deformation and costs elastic energy, which counteracts the NP–cell adhesion energy, presenting resistance to endocytosis. In the case that benign and malignant cells appreciably differ in their surface mechanics,<sup>[14]</sup> targeting specificity and selectivity could be further improved by biasing toward the surface mechanics of malignant cells. Further, some measures such as administering drugs or altering the local environment of cells and tissues can be taken to tune the surface mechanics of cells, thereby facilitating cellular uptake. The biased uptake based on differential cell surface mechanics could formulate a new targeting strategy, termed here mechanotargeting.

Herein, we carry out in vitro experiments to demonstrate the working principle of mechanotargeting. Noting that surface mechanics is a measure of the mechanical states of cells and ties with cell stress,<sup>[15–17]</sup> we correlate cell stress with cellular uptake in this study. As cells are able to sense and respond to their surrounding mechanical cues by subcellular structure remodeling, we direct cells into different stress states by seeding two cell lines, human cervical cancer (HeLa) cells and human colon carcinoma (HCT-8) cells, on hydrogels of different stiffness. Upon prolonged culture on relatively stiff hydrogels, HCT-8 cells undergo in vitro metastasis and malignant transformation, which offers a unique model for comparative study of the targeting efficiency to benign and malignant counterparts of the same cell type. For nonmetastatic cells, stiff hydrogels induce high cell stress as well as exposed surface area, and

Q. Wei, Dr. C. J. Huang, Dr. Y. Zhang, T. K. Zhao, P. Zhao, Prof. S. L. Zhang  
Department of Engineering Science and Mechanics  
Pennsylvania State University  
University Park  
PA 16802, USA  
E-mail: suz10@psu.edu

Prof. P. Butler, Prof. S. L. Zhang  
Department of Biomedical Engineering  
Pennsylvania State University  
University Park  
PA 16802, USA

 The ORCID identification number(s) for the author(s) of this article can be found under <https://doi.org/10.1002/adma.201707464>.

DOI: 10.1002/adma.201707464

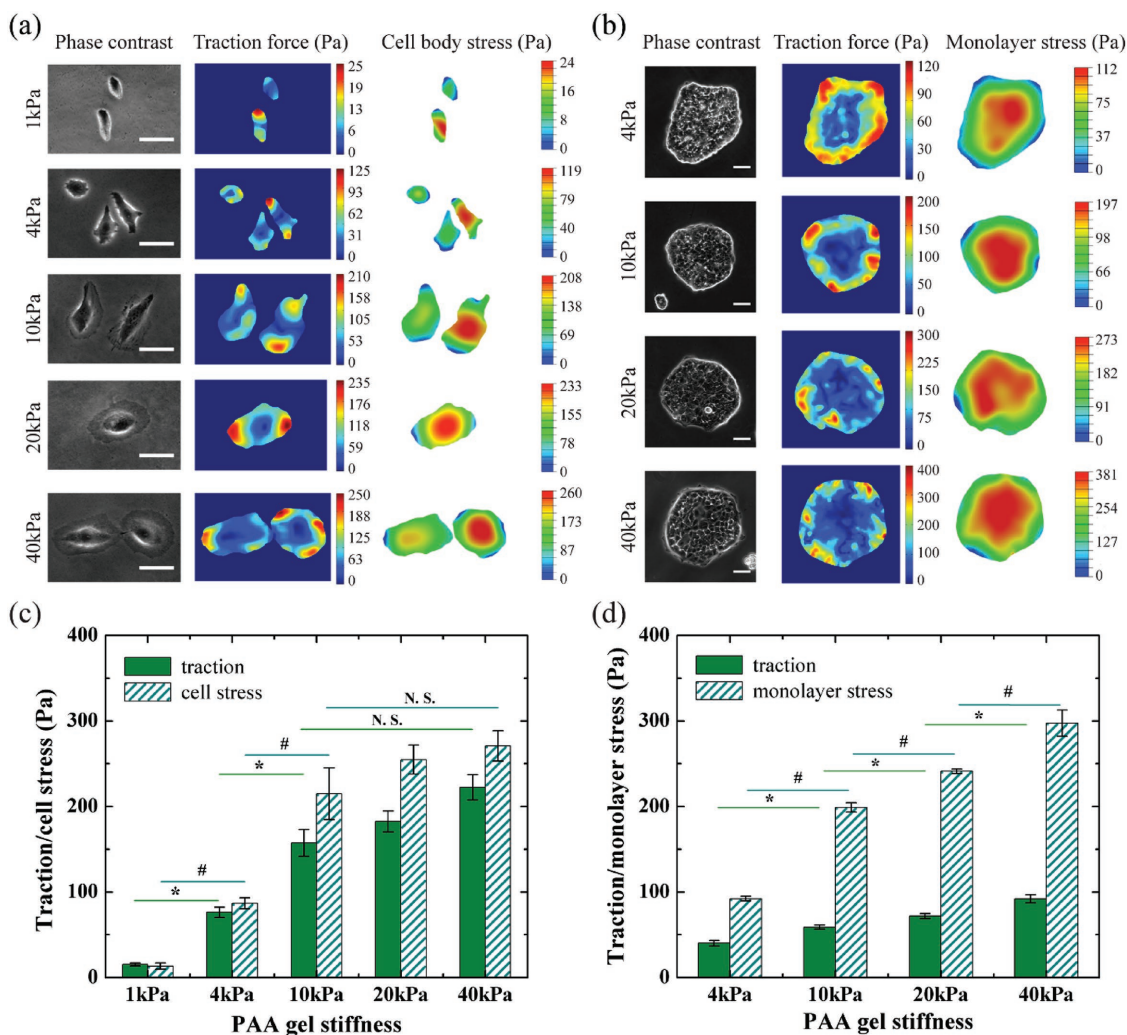


**Figure 1.** Traction force and cell stress for cells cultured on PAA hydrogels of different stiffness. a,c) Individual HeLa cells ( $n > 8$  for each condition); b,d) HCT-8 cell colonies ( $n > 5$  for each condition). Scale bar: 50  $\mu\text{m}$ . Data are presented as mean  $\pm$  SEM. \*  $p < 0.05$ ; #  $p < 0.05$ ; N.S. (no significant difference)  $p > 0.05$ .

these two factors counteract each other in determining the cellular uptake efficiency. Whereas metastatic HCT-8 cells exhibit increased exposed surface area and reduced cell stress, both favor cellular uptake and lead to fivefold increase in cellular uptake as compared to their nonmetastatic counterparts. Our finding underscores the importance of cell mechanical states in the design of highly efficient NP-based therapeutic and diagnostic agents.

Figure 1 shows that the two cell lines are directed into different stress states by culturing them on polyacrylamide (PAA) hydrogels of varying stiffness. The surface of the PAA gels is coated with fibronectin. The density of fibronectin is independent of gel stiffness,<sup>[18–20]</sup> which eliminates possible bias in cellular uptake of NPs due to different gel surface chemistries. Stiffness sensing of the cells activates a cascade of biochemical signals that regulate cytoskeletal remodeling, focal adhesion formation, and morphogenesis.<sup>[21–24]</sup> These intracellular and extracellular activities alter the stress state of cells.<sup>[25]</sup> Consistent with previous observations,<sup>[26]</sup> the spreading area of

individual HeLa cells increases with increasing substrate stiffness. Within several hours of culture, HCT-8 cells aggregate to form multicellular cohesive colonies, while HeLa cells remain separated and individuals in isolation. On soft hydrogels (<4 kPa), the HCT-8 cell colonies tend to form double layers, particularly at the boundary (Figure S1a, Supporting Information). As gel stiffness increases, the cell colonies exhibit monolayer morphology (Figure S1b,c, Supporting Information).

Adherent cells pull the substrate through focal adhesion points, generating traction (force per unit area) on the gel surface. The traction force reacts back to the cells, generating cell stress. We measure cell traction force by traction force microscopy<sup>[27,28]</sup> (TFM) and cell stress by monolayer stress microscopy<sup>[29]</sup> (MSM, see the Supporting Information). TFM involves embedding fluorescent beads into the hydrogels to track the displacement caused by the traction. The measured displacement field along with the materials properties of the hydrogels furnishes an inverse mechanics problem to calculate the traction force. Imposing force balance on the cell or

the cell sheet gives rise to the cell stress. Figure 1a shows that traction force is concentrated at the outer boundary of HeLa cells, consistent with the previously reported traction landscapes for single cells.<sup>[19,30]</sup> The measured cell stress is nearly uniform at the interior of the cells. Similar traction force and cell stress landscapes are observed for cohesive HCT-8 cell colonies (Figure 1b) despite the fact that each colony consists of hundreds of cells. Immunostaining of focal adhesion kinase (FAK) shows that the traction force is colocalized with focal adhesion points at the boundaries of the cell colonies (Figure S2, Supporting Information). For HeLa cells, we average the traction force and cell stress over the whole cell spreading area. For HCT-8 cell colonies, we average the traction force over the boundary layer ( $\approx 50 \mu\text{m}$ ), and the cell stress over the interior regions of nearly uniform stress. We take the different averaging schemes for HeLa cells and HCT-8 cell colonies for better correlation of cell stress with the cellular uptake of NPs, described later. In general, the average traction force and cell stress increase with hydrogel stiffness for both cell types (Figure 1c,d). For HeLa cells, traction force and cell stress reach a plateau beyond a gel stiffness of 10 kPa.

Cell morphologies and stress fiber assemblies are indicative of the stress states of cells.<sup>[31,32]</sup> Figure 2a shows that HeLa cells on 1 kPa gels round up and exhibit discrete F-actin, with very few stress fibers formed. With increasing hydrogel stiffness, particularly for stiffness greater than 10 kPa, cells spread and assemble F-actin filaments into thick, aligned stress fibers. These observations agree well with previous studies.<sup>[18,32]</sup> As gel stiffness increases, the F-actin filaments of HCT-8 colonies are also much thicker at the boundary, more aligned at basal surface and enriched at cell–cell junctions at apical surface (Figure 2b). Beyond a gel stiffness of 10 kPa, both cell lines exhibit insignificant morphological changes. We measured the exposed surface area of cells (see detailed method in the Supporting Information), defined as the portion of the accessible cell surface to NPs. The portion of cell surface that adheres to the gels or to the neighboring cells is inaccessible to NPs, and thus is not counted as part of the exposed surface area. As HeLa cells adopt different shapes on gels of different stiffness, we measure the exposed surface area by reconstructing the cell surface profile from 3D confocal scans (Figure 2c, insets). For cohesive HCT-8 cell colonies, the projected spreading area of

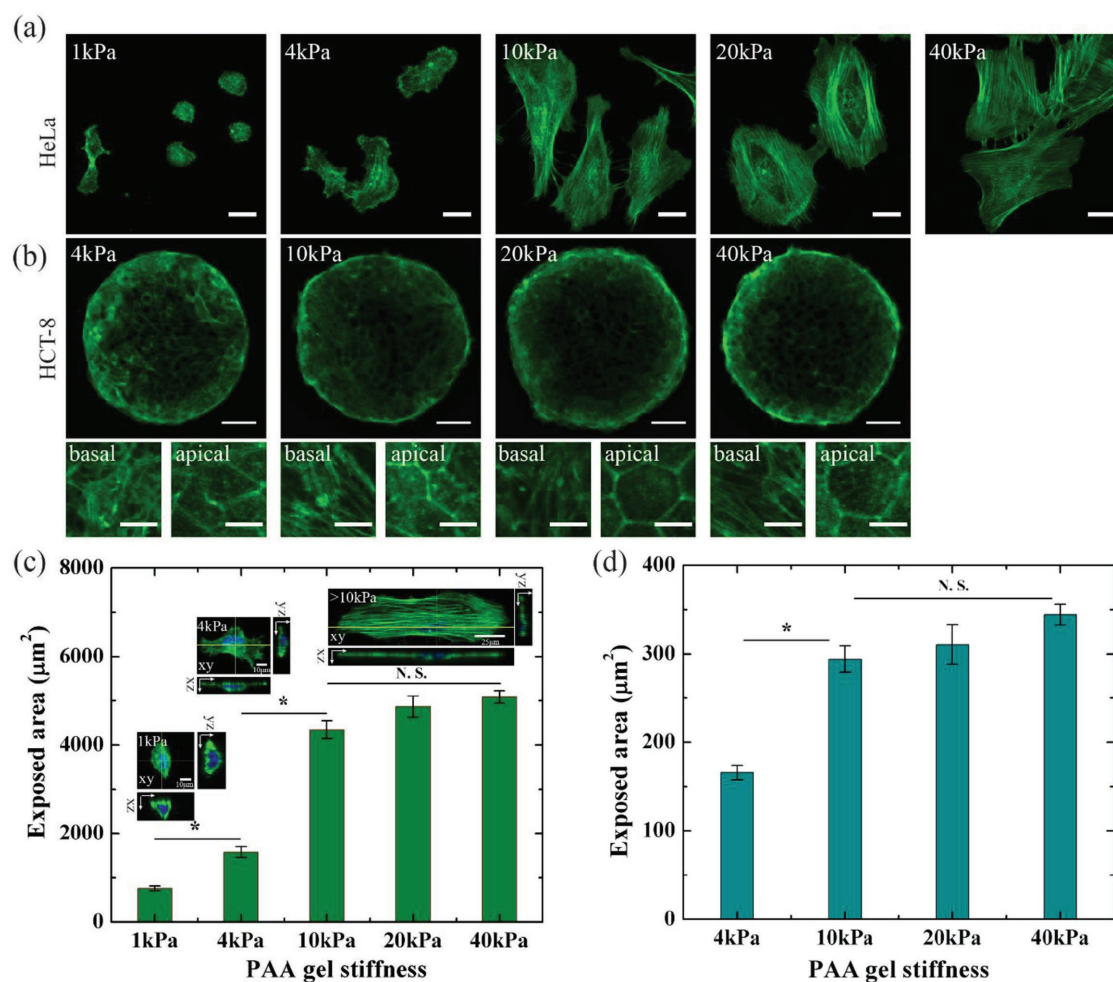


**Figure 2.** a,b) Cell morphology and stress fiber assembly on PAA hydrogels of different stiffness. Scale bar: first row ( $20 \mu\text{m}$ ); second row ( $50 \mu\text{m}$ ); third row ( $10 \mu\text{m}$ ). Statistical analysis of the effect of gel stiffness on the exposed area of cells to NPs: c) HeLa cells ( $n > 20$ ); d) HCT-8 cells ( $n > 10$ ). Insets in (c): 3D confocal scans of HeLa cell shapes. Data are presented as mean  $\pm$  SEM. \*  $p < 0.05$ ; N.S. (no significant difference)  $p > 0.05$ .

the cells at the colony interior approximates the exposed surface area since cell–cell adhesions block the side surface of the cells. For both cell types, the measured exposed surface area first increases and then levels off beyond a gel stiffness of 10 kPa (Figure 2c,d).

To correlate cell stress states to the cellular uptake of NPs, monodispersed carboxylate-modified polystyrene NPs (PS-COOH NPs) with diameter of 100 nm are used to target the two cell lines. The NPs encapsulate minimal photobleaching fluorescent dyes and the fluorescence intensity is positively correlated with the concentration of NPs. In the absence of surface ligands on the NPs, the adhesion energy driving endocytosis primarily arises from nonspecific interactions.<sup>[7,11]</sup> No obvious changes in either cell morphology or cell stress state were observed in the presence of NPs (Figure S3, Supporting Information). To remove the NPs in solution and adhered to cell surfaces, we thoroughly rinsed the cells three times with DPBS before extracting the cellular uptake of NPs. 3D confocal scans confirm that the fluorescence intensity of NPs is exclusively

from the internalized NPs (Figure S4, Supporting Information). In particular, the fluorescent signals of NPs in the 3D scans are found to fall within the cell boundary, traced by the immunostaining of F-actins. For HCT-8 cell colonies, fluorescence intensity is nearly uniform at the interior region, which is lower than that at the boundary layer (Figure 3b). This fluorescence intensity profile is consistent with the cell stress map shown in Figure 1, suggesting the strong negative correlation between cell stress and NP uptake density. For individual HeLa cells, the majority of internalized NPs agglomerates around cell nuclei rather than cell periphery (Figure 3a), despite the fact that the measured cell stress is higher at the cell interior. This is likely due to the intracellular trafficking of internalized NPs.<sup>[33]</sup> Though PS-COOH NPs may enter cells through both clathrin/caveolin-mediated and clathrin/caveolin-independent endocytosis pathways,<sup>[34,35]</sup> cellular uptake of NPs still involves cell membrane wrapping of nanoparticles (see details of the energetic of NP–cell interaction in the Supporting Information). As such, cell stress state remains a key regulating factor

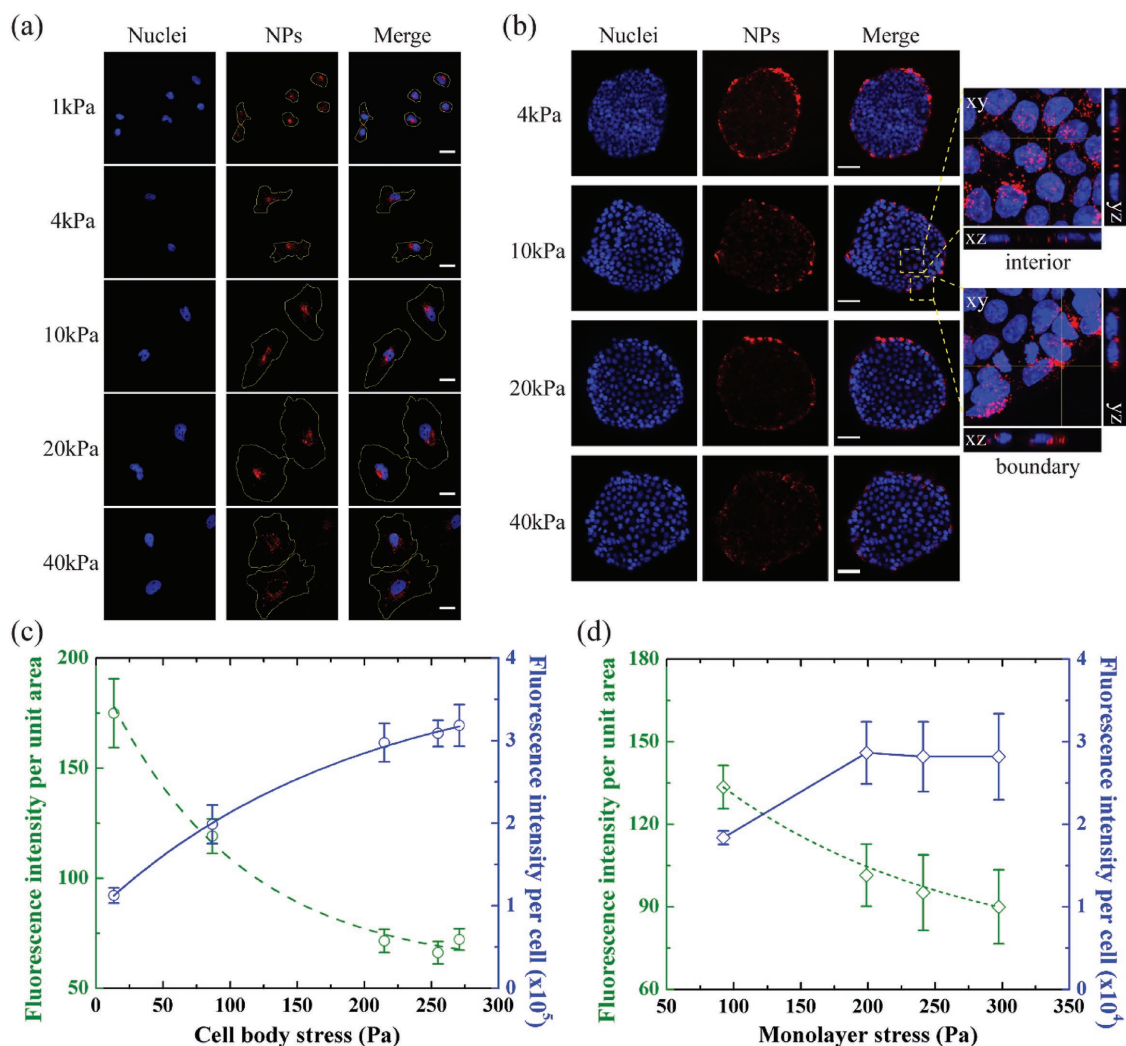


**Figure 3.** Correlation of cellular uptake and cell stress. Cells were cultured on PAA hydrogels of different stiffness for 24 h, followed by NPs loading and continuous culture for 8 h. a) HeLa, scale bar: 25  $\mu\text{m}$ ; b) HCT-8, scale bar: 50  $\mu\text{m}$ . Correlation of cell stress and cellular uptake on a per-cell-area and a per-cell basis: c) HeLa cells; d) HCT-8 cells. Data are presented as mean  $\pm$  SEM.

on the cellular uptake by affecting the deformation energy of membrane wrapping.

Previous theoretical analysis revealed that cellular uptake linearly scales with the exposed surface area of the cells.<sup>[12,13]</sup> To separate the effects of cell stress state and the exposed surface area, we quantify the cellular uptake on a per-cell basis ( $N$ ) and per-cell-area basis (i.e., areal density of uptake,  $N/A$ , where  $A$  is the exposed surface area of the cell) following a unified method (see details of the NP uptake assay in the Supporting Information). For HCT-8 cell colonies, we only measure the uptake of the interior cells so as to correlate the uptake with the nearly uniform stress therein. Figure 3c,d shows that with increasing average cell stress, cellular uptake on a per-cell-area basis decreases and then saturates, demonstrating that cell stress suppresses cellular uptake. This result is consistent with the biophysical analysis.<sup>[13]</sup> However, cellular uptake on a per-cell basis generally increases with increasing average stress for both cell lines. For HCT-8 cells, cellular uptake saturates beyond a monolayer stress of 200 Pa. This does not mean that cell stress promotes cellular uptake. Instead, with increasing cell stress, cells are more spread, giving rise to increased exposed surface area that is accessible to NPs (Figure S5, Supporting Information). Since the exposed surface area promotes cellular uptake

and the areal effect is dominant over the inhibiting effect of cell stress, this leads to high cellular uptake on a per-cell basis.

We have shown that for nonmetastatic adherent cells the exposed surface area counteracts with the stress state of cells in determining the cellular uptake of NPs. Next, we perform a comparative study of the cellular uptake of metastatic and nonmetastatic cells. HCT-8 cell colonies upon prolonged culture on stiff substrates (>20 kPa) progressively gain metastatic potential, and eventually disperse to individual malignant cells, featuring an in vitro metastatic-like phenotypic change.<sup>[36]</sup> The dispersion starts from the periphery of the cell colonies at  $\approx$ day 6 of culture (Figure 4d) and gradually propagates to the center. Upon 10 d of culture the cell colonies are all dispersed into individual, highly mobile and invasive cells (Figure 4a). The malignant phenotype is manifested by the irregularly shaped nuclei and reduced E-cadherin expression at cell–cell junctions,<sup>[36]</sup> both are hallmarks of invasive phenotype. The metastatic phenotypic change provides a comparative model for NP-targeting efficiency for cells with different states of malignancy. The dispersion was mediated by the spatiotemporal evolution of traction force and cell stress. In the predispersed stage, HCT-8 cell colonies feature a stress pattern depicted in Figure 4a (also shown in Figure 1b). Upon dispersion, traction force of the

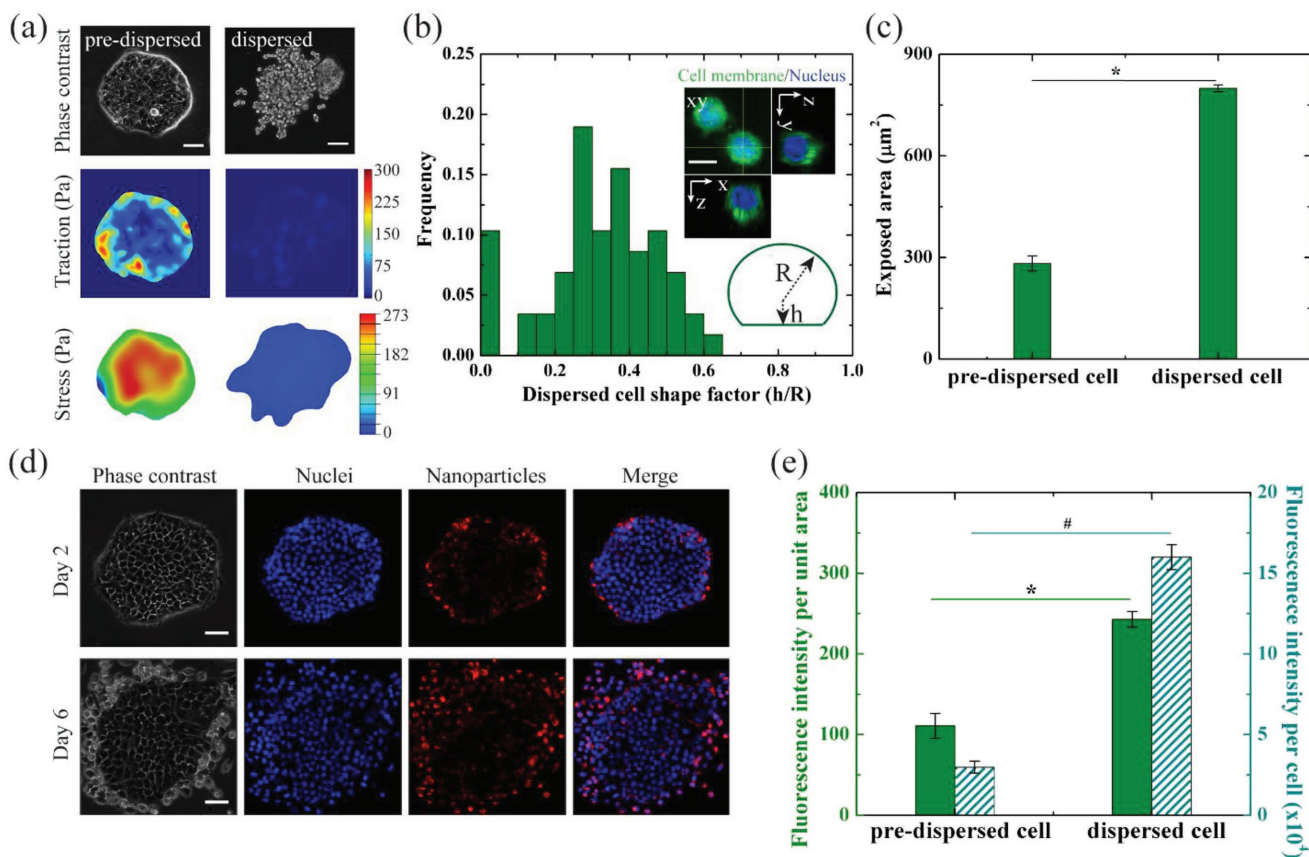


**Figure 4.** Cellular uptake of the HCT-8 cells before and after dispersion. a) Traction force and cell stress evolution of HCT-8 cell colonies grown on 20 kPa PAA gels at day 2 (predispersed) and day 10 (dispersed) of culture. b) Statistical analysis of the shape factor of dispersed cells. c) The exposed surface area of predispersed and dispersed cells. Data are presented as mean  $\pm$  SEM. d) NPs targeting HCT-8 cell colonies cultured on 20 kPa PAA gels at day 2 (predispersed) and day 6 (dispersed) of culture. Scale bar: 50  $\mu$ m. e) Cellular uptake of dispersed cells is  $\approx$ 2 times higher than predispersed cells on a per-cell-area basis, and  $\approx$ 5 times on a per-cell basis. \*  $p < 0.05$ ; #  $p < 0.05$ .

cell colonies diminishes, as does colony stress (Figure 4a). The dispersed cells are much softer than the predispersed ones, manifested by a much lower bending modulus and membrane tension,<sup>[37]</sup> consistent with the lower cell stress measured here. 3D confocal scans show that the dispersed individual cells exhibit heterogeneous shapes, characterized by  $h/R$  defined in the inset in Figure 4b. Different from HeLa cells for which the exposed surface area scales with cell stress, the dispersed cells, though with diminishing cell stress, have an exposed surface area of nearly threefold larger than the predispersed cells, as seen in Figure 4c. This difference arises because once the HCT-8 cells undergo metastatic phenotypic change, they no longer spread onto the 2D surface, but take a 3D morphology. Figure 4d,e shows the cellular uptake of the predispersed (non-metastatic) and dispersed (metastatic) cells. Cellular uptake of the dispersed cells is  $\approx 2$  times higher than that of the predispersed cells on a per-cell-area basis, and  $\approx 5$  times higher on a per-cell basis. The significantly biased uptake is due to both reduced cell stress and increased exposed area of the dispersed cells compared to the predispersed cells.

We conclude by noting that cellular uptake can be biased toward the cell stress states, enabling mechanotargeting, in distinct contrast to the conventional chemotargeting that relies on enhanced NP–cell adhesion specificity. To demonstrate the working principle of mechanotargeting, we direct the cells into different stress states and morphologies by seeding the cell lines on hydrogels of various stiffness. For nonmetastatic cells, cell stress and exposed surface area are both positively correlated with gel stiffness, and cell stress counteracts the exposed surface area in regulating cellular uptake. As the areal effect is more predominant, cellular uptake decreases on a per-cell-area basis but increases on a per-cell basis with increasing gel stiffness. Upon malignant transformation, dispersed, metastatic HCT-8 cells become much less stressed, and have a much larger exposed surface area than the nonmetastatic counterparts, both favoring cellular uptake. As a result, cellular uptake of the dispersed, malignant cells is fivefold higher than the predispersed cells.

Numerous studies have shown that normal and diseased cells markedly differ in their mechanical properties,<sup>[38–41]</sup> suggesting broader applications of mechanotargeting. For example, metastatic cells have been found to be substantially softer than benign cells;<sup>[38,39]</sup> cells grown under atherogenic conditions are substantially softer than cells grown under atheroprotective conditions;<sup>[40]</sup> malaria parasite-infected erythrocytes are significantly stiffer than healthy ones.<sup>[41]</sup> Here, we show that using the same NPs, cellular uptake is strongly biased to the metastatic, malignant cells because of their low cell stress and large exposed surface area as compared to their nonmetastatic, benign counterparts. To activate mechanotargeting in stiff high-stressed malignant cells, one may first chemically reduce the stress state, for example, by adding myosin contraction inhibitor,<sup>[35,42]</sup> or by altering the local environment of the cells,<sup>[43,44]</sup> as demonstrated here. Additionally, one may optimize NP size<sup>[45,46]</sup> or change the stiffness of NPs<sup>[47–49]</sup> to improve mechanotargeting, as it modulates the deformation energy of the cell membrane.<sup>[13]</sup> Nevertheless, our study exemplifies how mechanics can be harnessed to transform the future of nanomedicine, which may find broader applications in targeting a variety of mechanotransduction pathways of cells.

## Experimental Section

**Preparation of PAA Hydrogel Substrates:** PAA hydrogel substrates with controlled stiffness were fabricated following previously published protocols.<sup>[50]</sup> Briefly, 35  $\mu\text{L}$  prepolymerized solution with initiators (0.8  $\mu\text{L}$  TEMED and 2.5  $\mu\text{L}$  10% (w/v) ammonium persulfate) and following relative concentrations of acrylamide and bis-acrylamide: 5%/0.03% ( $1.0 \pm 0.3$  kPa), 5%/0.1% ( $4.0 \pm 0.8$  kPa), 8%/0.13% ( $10.0 \pm 1.6$  kPa), 8%/0.27% ( $20.0 \pm 1.2$  kPa), and 8%/0.48% ( $40.4 \pm 2.4$  kPa), was sandwiched between an amino-activated coverslip (diameter 25 mm, VWR International) and a Rain-X treated hydrophobic glass slide. After polymerization, PAA gel bound to the activated coverslip was detached from the glass slide and sequentially activated with 0.5  $\text{mg mL}^{-1}$  Sulfo-SANPAH (Pierce Chemical) under 365 nm UV light, functionalized with fibronectin (Sigma Aldrich) at a concentration of 0.05  $\text{mg mL}^{-1}$  for overnight and sterilized in a biological cabinet before cell seeding.

**Cell Culture:** HeLa cells and HCT-8 cells (ATCC) were seeded onto PAA gel substrates at a density of 10 000 cells  $\text{cm}^{-2}$  and cultured for 48 h in DMEM medium supplemented with 10% fetal bovine serum and RPMI-1640 medium supplemented with 10% nonheat inactivated horse serum, respectively, at 37 °C in 5%  $\text{CO}_2$  atmosphere. In the metastatic-like dispersion experiment, HCT-8 colonies were cultured on 20 kPa gel substrates for at least 6 d with cell medium changed every other day.

**Traction Force Microscopy:** To measure cell traction force, fluorescent beads (200 nm in diameter, Life Technologies) were placed on a single plane beneath PAA gel surface following a previously published protocol,<sup>[50]</sup> being a tracer of the gel deformation. A phase contrast image of a selected HeLa cell or HCT-8 colony and a pair of fluorescent images of beads taken before and after cells were detached from the gel were collected. The lateral movement of beads extracted from the paired images gave rise to the in-plane displacement field of the gel. The corresponding traction force profile was obtained by solving the inverse elasticity problem furnished by the displacement field along with the boundary conditions based on Boussinesq solution.

**Monolayer Stress Microscopy:** To analyze the cell stress of both cell lines, MSM<sup>[29]</sup> was implemented. Briefly, the cell geometries from the phase contrast images were meshed. The traction force profiles derived from TFM were converted into the body force and used as a boundary condition. Treating cells as a linear elastic material, solving the 2D boundary value problem in elasticity with the finite element package (ABAQUS) gave rise to the cell stress.

**NPs Uptake Assay:** Carboxylate-modified fluorescent polystyrene NPs (100 nm in diameter, Ex/Em: 580/605 nm) were sonicated for 15 min to avoid possible aggregations, then diluted in fresh cell medium to reach a final concentration of 0.02  $\text{mg mL}^{-1}$  and incubated with cells. After 8 h incubation, cells were thoroughly rinsed three times with DPBS, fixed with 4% paraformaldehyde solution, stained with AlexFluor488 phalloidin for F-actin filaments and DAPI for nuclei. All materials were purchased from Life Technologies. In single HeLa cell experiments, z-stacked images were taken using a confocal fluorescence microscope (Olympus FV10i, Japan) with a 60 $\times$  water-immersion lens (NA = 1.2, Olympus, Japan). In HCT-8 cell colonies experiments, images were taken with a 20 $\times$  lens (NA = 0.4, Olympus, Japan). All images were collected with the same exposure parameters (e.g., laser intensity, exposure time, sensitivity of CCD). Detailed method describing the analysis of cell exposed surface area and NPs uptake is provided in the Supporting Information.

**Statistics:** Statistical analysis was performed in OriginPro 8.0 using Student's two-tailed *t*-test between any two data sets. Data are presented as mean  $\pm$  standard error of the mean (SEM). Significance level is set as  $p < 0.05$ , where  $p > 0.05$  is considered as no statistically significant difference. Sample size is shown in each figure and data are from at least three parallel experiments.

## Supporting Information

Supporting Information is available from the Wiley Online Library or from the author.

## Acknowledgements

S.L.Z. gratefully acknowledges supports from the National Science Foundation (NSF) grants (CMMI-0754463/0644599 and CBET-1067523). Both S.L.Z. and P.B. would like to acknowledge the support by the National Institutes of Health (NIH-NHLBIR21 HL122902).

## Conflict of Interest

The authors declare no conflict of interest.

## Keywords

cell stress, drug delivery, mechanotargeting, metastatic cells, nanoparticles

Received: December 21, 2017

Revised: April 7, 2018

Published online:

- 
- [1] M. Ferrari, *Nat. Rev. Cancer* **2005**, *5*, 161.
- [2] D. Peer, J. M. Karp, S. Hong, O. C. Farokhzad, R. Margalit, R. Langer, *Nat. Nanotechnol.* **2007**, *2*, 751.
- [3] M. E. Davis, D. M. Shin, *Nat. Rev. Drug Discovery* **2008**, *7*, 771.
- [4] I. Brigger, C. Dubernet, P. Couvreur, *Adv. Drug Delivery Rev.* **2002**, *54*, 631.
- [5] H. Otsuka, Y. Nagasaki, K. Kataoka, *Adv. Drug Delivery Rev.* **2012**, *64*, 246.
- [6] L. C. Kennedy, L. R. Bickford, N. A. Lewinski, A. J. Coughlin, Y. Hu, E. S. Day, J. L. West, R. A. Drezek, *Small* **2011**, *7*, 169.
- [7] A. E. Nel, L. Madler, D. Velegol, T. Xia, E. M. V. Hoek, P. Somasundaran, F. Klaessig, V. Castranova, M. Thompson, *Nat. Mater.* **2009**, *8*, 543.
- [8] S. Wilhelm, A. J. Tavares, Q. Dai, S. Ohta, J. Audet, H. F. Dvorak, W. C. Chan, *Nat. Rev. Mater.* **2016**, *1*, 16014.
- [9] B. Pelaz, C. Alexiou, R. A. Alvarez-Puebla, F. Alves, A. M. Andrews, S. Ashraf, L. P. Balogh, L. Ballerini, A. Bestetti, C. Brendel, S. Bosi, M. Carril, W. C. W. Chan, C. Chen, X. Chen, X. Chen, Z. Cheng, D. Cui, J. Du, C. Dullin, A. Escudero, N. Feliu, M. Gao, M. George, Y. Gogotsi, A. Grünweller, Z. Gu, N. J. Halas, N. Hampp, R. K. Hartmann, M. C. Hersam, P. Hunziker, J. Jian, X. Jiang, P. Jungebluth, P. Kadhiresan, K. Kataoka, A. Khademhosseini, J. Kopeček, N. A. Kotov, H. F. Krug, D. S. Lee, C.-M. Lehr, K. W. Leong, X.-J. Liang, M. L. Lim, L. M. Liz-Marzán, X. Ma, P. Macchiarelli, H. Meng, H. Möhwald, P. Mulvaney, A. E. Nel, S. Nie, P. Nordlander, T. Okano, J. Oliveira, T. H. Park, R. M. Penner, M. Prato, V. Punties, V. M. Rotello, A. Samarakoon, R. E. Schaak, Y. Shen, S. Sjöqvist, A. G. Skirtach, M. G. Soliman, M. M. Stevens, H.-W. Sung, B. Z. Tang, R. Tietze, B. N. Udugama, J. S. VanEpps, T. Weil, P. S. Weiss, I. Willner, Y. Wu, L. Yang, Z. Yue, Q. Zhang, Q. Zhang, X.-E. Zhang, Y. Zhao, X. Zhou, W. J. Parak, *ACS Nano* **2017**, *11*, 2313.
- [10] H. Gao, W. Shi, L. B. Freund, *Proc. Natl. Acad. Sci. USA* **2005**, *102*, 9469.
- [11] S. Zhang, H. Gao, G. Bao, *ACS Nano* **2015**, *9*, 8655.
- [12] H. Yuan, J. Li, G. Bao, S. Zhang, *Phys. Rev. Lett.* **2010**, *105*, 138101.
- [13] S. Zhang, J. Li, G. Lykotrafitis, G. Bao, S. Suresh, *Adv. Mater.* **2009**, *21*, 419.
- [14] S. E. Cross, Y. S. Jin, J. Rao, J. K. Gimzewski, *Nat. Nanotechnol.* **2007**, *2*, 780.
- [15] A. G. Clark, O. Wartlick, G. Salbreux, E. K. Paluch, *Curr. Biol.* **2014**, *24*, 484.
- [16] A. Bretscher, K. Edwards, R. G. Fehon, *Nat. Rev. Mol. Cell Biol.* **2002**, *3*, 586.
- [17] S. Tee, J. Fu, C. S. Chen, P. A. Janmey, *Biophys. J.* **2011**, *100*, L25.
- [18] T. Yeung, P. C. Georges, L. A. Flanagan, B. Marg, M. Ortiz, M. Funaki, N. Zahir, W. Y. Ming, V. Weaver, P. A. Janmey, *Cell Motil. Cytoskeleton* **2005**, *60*, 24.
- [19] A. Elosegui-Artola, R. Oria, Y. F. Chen, A. Kosmalska, C. Perez-Gonzalez, N. Castro, C. Zhu, X. Trepas, P. Roca-Cusachs, *Nat. Cell Biol.* **2016**, *18*, 540.
- [20] R. J. Pelham, Y. L. Wang, *Proc. Natl. Acad. Sci. USA* **1997**, *94*, 13661.
- [21] N. Wang, J. P. Butler, D. E. Ingber, *Science* **1993**, *260*, 1124.
- [22] C. S. Chen, J. Tan, J. Tien, *Annu. Rev. Biomed. Eng.* **2004**, *6*, 275.
- [23] D. E. Discher, P. Janmey, Y. L. Wang, *Science* **2005**, *310*, 1139.
- [24] X. Cao, Y. Lin, T. P. Driscoll, J. Franco-Barraza, E. Cukierman, R. L. Mauck, V. Shenoy, *Biophys. J.* **2016**, *110*, 1807.
- [25] J. T. Parsons, A. R. Horwitz, M. A. Schwartz, *Nat. Rev. Mol. Cell Biol.* **2010**, *11*, 633.
- [26] S. Zustiak, R. Nossal, D. L. Sackett, *Biotechnol. Bioeng.* **2014**, *111*, 396.
- [27] J. P. Butler, I. M. Tolić-Nørrelykke, B. Fabry, J. J. Fredberg, *Am. J. Physiol.* **2002**, *282*, C595.
- [28] Q. Tseng, E. Duchemin-Pelletier, A. Deshieri, M. Balland, H. Guillou, O. Filhol, M. Théry, *Proc. Natl. Acad. Sci. USA* **2012**, *109*, 1506.
- [29] D. T. Tambe, C. C. Hardin, T. E. Angelini, K. Rajendran, C. Y. Park, X. Serra-Picamal, E. H. Zhou, M. H. Zaman, J. P. Butler, D. A. Weitz, *Nat. Mater.* **2011**, *10*, 469.
- [30] U. S. Schwarz, M. L. Gardel, *J. Cell Sci.* **2012**, *125*, 3051.
- [31] S. Tavares, A. F. Vieira, A. V. Taubenberger, M. Araújo, N. P. Martins, C. Brás-Pereira, A. Polónia, M. Herbig, C. Barreto, O. Otto, *Nat. Commun.* **2017**, *8*, 15237.
- [32] S. Walcott, S. X. Sun, *Proc. Natl. Acad. Sci. USA* **2010**, *107*, 7757.
- [33] J. Gilleron, W. Querbes, A. Zeigerer, A. Borodovsky, G. Marsico, U. Schubert, K. Manygoats, S. Seifert, C. Andree, M. Stöter, *Nat. Biotechnol.* **2013**, *31*, 638.
- [34] Z. Mao, X. Zhou, C. Gao, *Biomater. Sci.* **2013**, *1*, 896.
- [35] T. d. Santos, J. Varela, I. Lynch, I. Salvati, K. A. Dawson, *PLoS One* **2011**, *6*, e24438.
- [36] X. Tang, T. B. Kuhlenschmidt, J. Zhou, P. Bell, F. Wang, M. S. Kuhlenschmidt, T. A. Saif, *Biophys. J.* **2010**, *99*, 2460.
- [37] X. Tang, T. B. Kuhlenschmidt, Q. Li, S. Ali, S. Lezmi, H. Chen, M. Pires-Alves, W. W. Laegreid, T. A. Saif, M. S. Kuhlenschmidt, *Mol. Cancer* **2014**, *13*, 131.
- [38] D. T. Butcher, T. Alliston, V. M. Weaver, *Nat. Rev. Cancer* **2009**, *9*, 108.
- [39] S. Kumar, V. M. Weaver, *Cancer Metastasis Rev.* **2009**, *28*, 113.
- [40] Y. S. J. Li, J. H. Haga, S. Chien, *J. Biomech.* **2005**, *38*, 1949.
- [41] Y. Zhang, C. Huang, S. Kim, M. Golkaram, M. W. Dixon, L. Tilley, J. Li, S. Zhang, S. Suresh, *Proc. Natl. Acad. Sci. USA* **2015**, *112*, 6068.
- [42] J. C. Martens, M. Radmacher, *Pflügers Arch. Eur. J. Physiol.* **2008**, *456*, 95.
- [43] C. Huang, P. J. Butler, S. Tong, H. S. Muddana, G. Bao, S. Zhang, *Nano Lett.* **2013**, *13*, 1611.
- [44] C. Huang, T. Ozdemir, L. C. Xu, P. J. Butler, C. A. Siedlecki, J. L. Brown, S. Zhang, *J. Biomed. Mater. Res., Part B* **2016**, *104*, 488.
- [45] B. D. Chithrani, A. A. Ghazani, W. C. W. Chan, *Nano Lett.* **2006**, *6*, 662.
- [46] W. Jiang, B. Y. S. Kim, J. T. Rutka, W. C. W. Chan, *Nat. Nanotechnol.* **2008**, *3*, 145.
- [47] X. Yi, X. Shi, H. Gao, *Phys. Rev. Lett.* **2011**, *107*, 098101.
- [48] Q. Feng, J. Liu, X. Li, Q. Chen, J. Sun, X. Shi, B. Ding, H. Yu, Y. Li, X. Jiang, *Small* **2017**, *13*, 1603109.
- [49] J. Sun, L. Zhang, J. Wang, Q. Feng, D. Liu, Q. Yin, D. Xu, Y. Wei, B. Ding, X. Shi, X. Jiang, *Adv. Mater.* **2015**, *27*, 1402.
- [50] S. G. Knoll, M. Y. Ali, M. Saif, *J. Vis. Exp.* **2014**, *91*, e51873.